行政院國家科學委員會補助專題研究計畫 ■成果報告

□期中進度報告

適用於光波導元件的有限差分數值模型之發展(1/3)

計畫類別：■ 個別型計畫　□ 整合型計畫

計畫編號：NSC90－2215－E－002－040

執行期間：90 年 8 月 1 日至 91 年 9 月 30 日

計畫主持人：張宏鈞

共同主持人：

計畫參與人員：江衍忠(台大電機系)　江彥青(台大光電所)

林邦彥(台大電信所)　蔡耀群(台大電信所)

吳勁龍(台大電信所)　黃永成(台大電信所)

成果報告類型(依經費核定清單規定繳交)：■精簡報告　□完整報告

本成果報告包括以下應繳交之附件：

□赴國外出差或研習心得報告一份

□赴大陸地區出差或研習心得報告一份

■出席國際學術會議心得報告及發表之論文各一份

□國際合作研究計畫國外研究報告書一份

處理方式：除產學合作研究計畫、提升產業技術及人才培育研究計畫、列管計畫及下列情形者外，得立即公開查詢

□涉及專利或其他智慧財產權，□一年□二年後可公開查詢

執行單位：國立台灣大學光電工程學研究所

中　華　民　國　九　十　一　年　十　二　月　三　十　一　日

行政院國家科學委員會專題研究計畫成果報告

適用於光波導元件的有限差分數值模型之發展(1/3)

Development of Finite Difference Numerical Models for Photonic Guided-wave Devices (1/3)

計畫編號：NSC 90-2215-E-002-040

執行期限：90 年 8 月 1 日至 91 年 9 月 30 日

主持人：張宏鈞　　台灣大學電機系、光電所暨電信所教授

計畫參與人員：江衍忠(台大電機系)　江彥青(台大光電所)

林邦彥(台大電信所)　蔡耀群(台大電信所)

吳勁龍(台大電信所)　黃永成(台大電信所)

一、中文摘要

本計畫改良並發展數種應用於研究各種光導波元件的有限差分數值模型，包括全向量有限差分模態分析模型之改良、時域波束傳播法之發展、彎曲光波導的三維全向量波束傳播分析、以及融燒式 3 × 3 光纖耦合器的繼續研究。第一年執行情形，依四項研究課題，分述於本報告。

關鍵詞：光波導、波導元件、有限差分法、波束傳播法、時域波束傳播法、時域有限差分法、光纖耦合器

Abstract

This research concerns improvement and development of several finite difference (FD) numerical models as tools for studying various photonic guided-wave devices, including improvement of our full-vectorial FD waveguide mode solver, development of time-domain beam propagation method (FD-BPM), generalization of our three-dimensional full-vectorial FD-BPM to analyzing curved optical waveguides, and continuous research on fused 3 × 3 fiber-optic couplers. The results of four topics of study obtained in the first phase of this research are briefly described respectively in this report.

Keywords: Optical waveguides, waveguide devices, finite difference method, beam propagation method, time-domain beam propagation method, finite difference time domain method, fiber-optic couplers

二、計畫緣由與目的

本計畫改良並發展數種有限差分數值模型，以做為研究各種光導波元件的工具。除了改良及應用分析及設計光導波結構常使用的有限差分波導模態求解模型以及有限差分波束傳播法模型外，並進一步發展可分析包括反射在內等更廣泛現象的時域波束傳播法模型。第一年執行情形，依全向量有限差分模態分析模型之改良、時域波束傳播法之發展、彎曲光波導的三維全向量波束傳播分析、融燒式 3 × 3 光纖耦合器的繼續研究等四項研究課題，分述於下。所引參考著作係已完成之期刊論文及研討會論文，其中一篇附於報告之後。

三、結果與討論

I. 全向量有限差分模態分析模型之改良：

有限差分法是分析介質波導模態最常用的方法之一，唯對於不同折射率介質接面上的邊界條件之處理方式是影響數值準確度的因素之一。早期的簡化處理方式乃是採用網格間的折射率平均，其準確度僅有 $O(h^0)$，其中 h 代表網格寬度，亦即再密的網格也無法增加準確度。如果將邊界條件加以匹配，準確度可增至 $O(h^2)$。先前我們針對截面折射率係一維的光波導，經由泰勒級數推導、匹配介面邊界條件、並採用 generalized Douglas scheme，推得準確可達 $O(h^4)$的有限差分三點公式。另外對於截面折射率為二維的光波導，例如階射率光纖，我們亦已經由匹配介面邊界條件建立收斂性較佳的全向量模態分析模型，可以採用較粗的網格，因之節省計算時間。上述模型係以磁場分量推得，在本年度中，我們建立了以電場分量為推導基礎的模型，並與磁場分量模型比較收斂特性。另外，先前的分析係假設所考慮的網格點之間的介質接面為平面，我們推導並建立介質接面為曲面的模型，進一步增加了數值效率。此研究結果發表於 Journal of Lightwave Technology [1]以及研討會[2], [3]，其中一部分結果請參附錄一[2]。

II. 時域波束傳播法之發展：

通常所用的(頻域)波束傳播法(BPM)僅能處理光波前向傳播的問題，雖然有所謂的雙向 BPM，我們先前也曾提出可利用 Pade approximants 分析光波導不連續的問題，但在使用上尚未具普遍性。因之，遇到有反射或其他散射現象存在的結構，另一可以採用的方法是 FDTD 法。FDTD 法雖是一項有力的技術，但它要求足夠細的網格以及時間步驟，因而是極耗用計算時間的方法。在訊號調制頻率極低於光載波頻率的情況下，時域波束傳播法(TD-BPM)是最近被提出的一項有效的方法，主要是在時間軸上提出光載波頻率項而僅分析緩慢變化的脈波波形，因之得以採用較大的時間步驟。在本年度中，我們著手建立 TE 波的時域二維 BPM，已有數值結果[4]，對於數值模型正持續改進中，並正進行更多數值實例的分析與探究。圖(一)為所考慮的板形介質波導不連續結構之一例，其四周加入 PML 吸收邊界，所用參數為 $d_1 = 1.458\mu m$，$d_2 = 14.58\mu m$，$d_3 = 10\mu m$，$n_1 = 3.6$，$n_2 = 4.0$，$n_3 = 3.564$，以導波模態之高斯脈衝由左側入射所獲得之透射與反射波延 z 方向的分布示於圖(二)(a)，其中實線為入射脈衝。圖(二)(b)為反射波的放大圖，其中不同曲線分別代表有與沒有處理介質邊界的結果。

III. 彎曲光波導的三維全向量波束傳播分析：

先前我們提出一項採用區域斜向座標的二維波束傳播法(LOC-BPM)以處理彎曲光波導的問題。針對計算區域中的每一(x, z)點，我們定義一個區域(ξ, ζ)座標，在區域座標上推導延著 z 方向第 s 步的場量Φ和第 s－1 步的場量的關係，然後將所有區域座標的關係式整合回 x-z 座標形成一個類似直角座標波束傳播法(RCS-BPM)的整體關係式，接下去的計算程序即和一般波束傳播法相同。我們隨後改良了 LOC-BPM，可以處理大角度甚至完整圓周彎曲波導中的光波傳播，在本年度中我們推展至三維波導結構的全向量場模擬。Table 1 為邊長為 $2\mu m$ 之彎曲正方形介質波導在不同曲率半徑 R 下，其傳播耗損率計算結果的比較，Improved LOC-BPM 指本研究所發展的方法，ESW 指 Equivalent Straight Waveguide 近似法。Table 2 為本研究所發展的方法之電場方法與磁場方法的比較。Table 3 為針對具不同凸出高度 d 之曲形脊形波導的傳播耗損率計算結果，NA 表示曲形波導無法導光，傳播耗損率極大。

IV. 融燒式 3 × 3 光纖耦合器的繼續研究：

我們繼續針對三根單模光纖排列所構成的 3 × 3 融燒式耦合器結構，利用邊界積

分法，進行準確的模態分析，計算傳播常數、耦合係數、相關的結構雙折性。根據我們先前對於 2 × 2 與 3 × 3 耦合器的研究經驗，發現利用邊界積分法解析時，如果採用均勻邊界分割，需要分割至數千段以上，才能獲得兩位有效數字的結構雙折性數值，計算量相當驚人，因而提出不均勻分割的方法，在邊界形狀的尖點附近，由於場量變化急劇，因此採用較密的分割，其餘部分則採用較疏的分割，得以節省大量的計算時間而仍得到可靠的準確度。由於電腦計算速度持續進步，使我們得以計算分割數更多的情況。而瞭解均勻邊界分割的確實收斂情形以驗證不均勻分割的方法的準確程度仍是相當重要的課題，在本研究中，我們將均勻分割數增至 3000，檢驗 2 × 2 與 3 × 3 耦合器的結構雙折性數值的收斂趨勢，分別示於圖(三)與圖(四)[5]。

四、計畫成果自評

本計畫研究內容與原計畫相符，預期目標大致達成。在全向量有限差分模態分析模型之改良方面，我們經由匹配介面邊界條件建立收斂性較佳的全向量模態分析模型，可以採用較粗的網格，因之節省計算時間，此結果已發表於 Journal of Lightwave Technology [1]。在時域波束傳播法之發展方面，已建立程式並應用於波導結構的透射反射問題，但由本研究經驗我們認為 FDTD 應為較合適的方法。在彎曲光波導的三維全向量波束傳播分析方面，我們分別建立了電場方法與磁場方法，並應用於有正方形介質波導與脊形波導之研究。最後，在融燒式 3 × 3 光纖耦合器的繼續研究方面，我們仔細檢驗 2 × 2 與 3 × 3 耦合器的結構雙折性數值隨邊界分割數的收斂趨勢，期獲得可信的數值。以上結果均具學術價值。

五、參考文獻

[1] Y. C. Chiang, Y. P. Chiou, and H. C. Chang, “Improved Full-Vectorial Finite-Difference Mode Solver for Optical Waveguides with Step-Index Profiles,” *IEEE/OSA Journal of Lightwave Technology*, Vol. 20, No. 8, pp. 1609–1618, August 2002.

[2] Y. C. Chiang and H. C. Chang, “Improved Full-Vectorial Finite-Difference Method for Waveguides with Curved Step-Index Profiles,” in *Proceedings of Optics and Photonics Taiwan '01 (OPT '01)*, Vol. I, pp. 143–145, Kaohsiung, Taiwan, R.O.C., December 13–14, 2001.

[3] Y. C. Chiang and H. C. Chang, “Full-Vectorial Finite-Difference Mode Solver for Optical Waveguides with corners,” accepted for presentation at *2002 Progress in Electromagnetics Research Symposium Proceedings (PIERS 2001)*, Cambridge, Massachusetts, U. S. A., July 1–5, 2002.

[4] B. Y. Lin and H. C. Chang, “On the Alternating Directional Implicit Method Applied in the Finite Difference Time Domain Beam Propagation Method,” in *Proceedings of Optics and Photonics Taiwan '02 (OPT '02)*, Vol. II, pp. 144–146, Taipei, Taiwan, R.O.C., December 12–13, 2002.

[5] Y. C. Tsai, B. R. Jiang, and H. C. Chang, “On the Convergence Characteristics of the Modal Analysis of Fused Fiber-Optic Couplers,” to be presented at *CLEO/PR 2003*, Taipei, Taiwan, R.O.C., 2003.

Table 1

Differential Loss Rates 2Γ $(10^3\mu m)^{-1}$ for Rectangular Waveguides Using Full-Vectorial Calculation
($\lambda = 1.55$ μm, $h_1 = h_2 = 2$ μm, $n_{core} = 1.45$, $n_{clad} = 1.55$)

$R(\mu m)$	ESW		Improved LOC-BPM	
	x-polarized	y-polarized	x-polarized	y-polarized
25	54.4000	52.0955	42.093	40.03691
50	7.1784	7.1296	6.5911	6.4304
75	1.0177	1.0034	1.011	0.98906
100	0.11913	0.1164	0.13352	0.12947

Table 2

Differential Loss Rates 2Γ $(10^3\mu m)^{-1}$ for Rectangular Waveguides Using Full-Vectorial Calculation
($\lambda = 1.55$ μm, $h_1 = h_2 = 2$ μm, $n_{core} = 1.45$, $n_{clad} = 1.55$)

$R(\mu m)$	H formula		E formula	
	x-polarized	y-polarized	x-polarized	y-polarized
25	42.342	40.3947	42.093	40.03691
50	6.628	6.4350	6.5911	6.4304
75	1.0183	0.9683	1.011	0.98906
100	0.13992	0.1383	0.13352	0.12947

Table 3

Differential Loss Rates 2Γ $(10^3\mu m)^{-1}$ for Rib Waveguides Using Full-Vectorial Calculation
($\lambda = 1.55$ μm, $n_{core} = 3.44$, $n_{sub} = 3.34$)

$R(\mu m)$	$d = 1$ μm		$d = 0.7$ μm		$d = 0.5$ μm	
Dominant field	H_y	H_x	H_y	H_x	H_y	H_x
25	8.556	9.7377	NA	NA	NA	NA
50	3.917	3.0108	16.210	17.421	NA	NA
75	1.379	1.1021	5.8737	6.3538	NA	NA
100	0.448	0.3084	1.9056	1.6539	12.575	16.267
150	0.0634	0.0489	0.2847	0.241	2.897	3.9106
200			0.0472	0.0395	0.652	1.0014

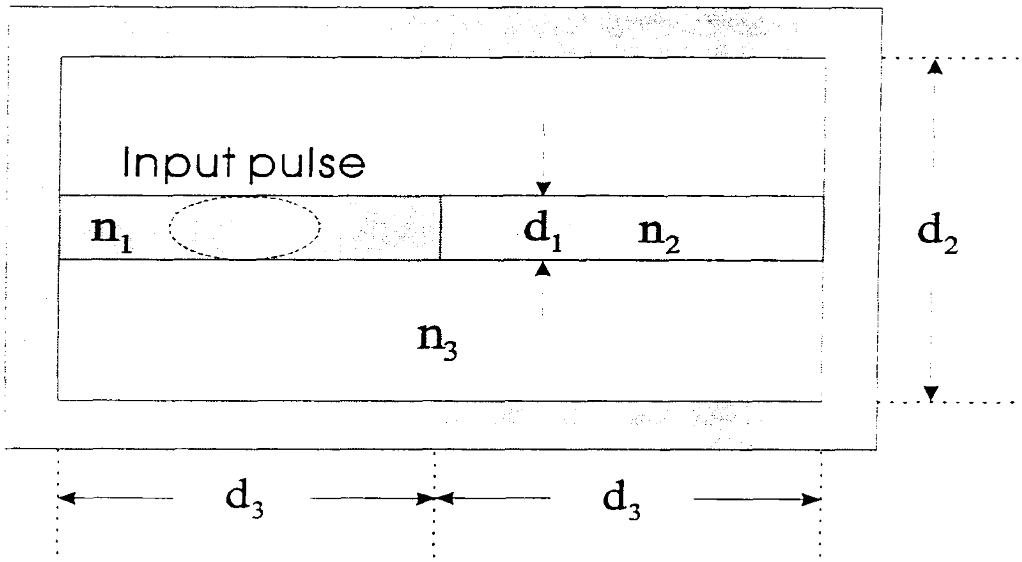

圖(一)　輸入脈衝在介質波導不連續結構傳播示意圖。

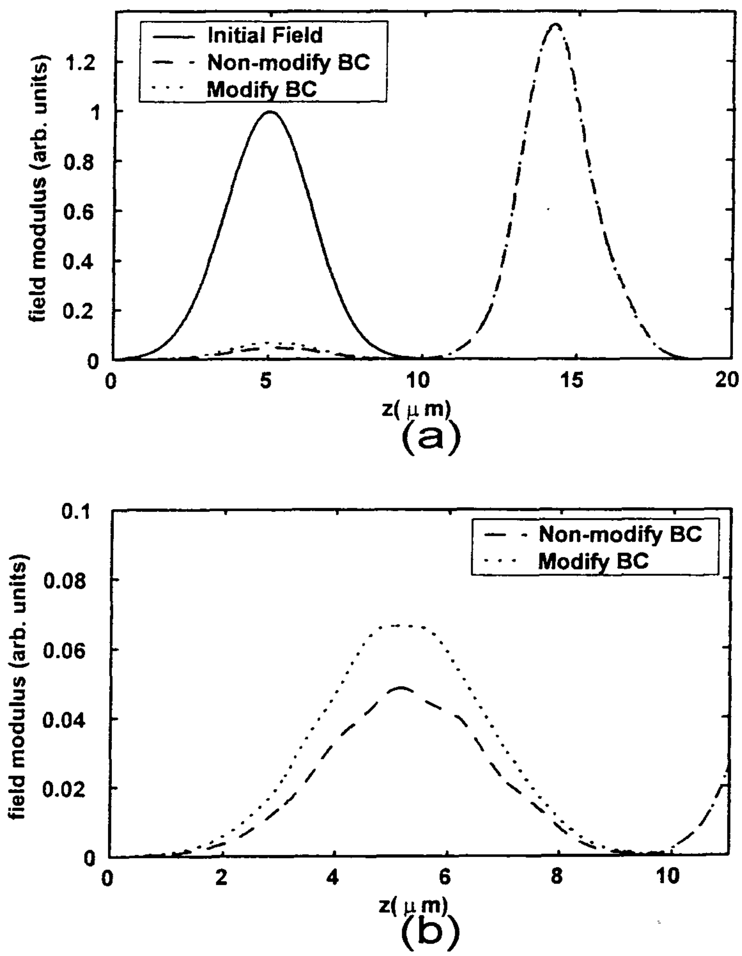

圖(二)　(a) 導波模態之高斯脈衝由左側入射所獲得之透射與反射波延z方向的分布圖。(b)反射波的放大圖，其中不同曲線分別代表有與沒有處理介質邊界的結果。

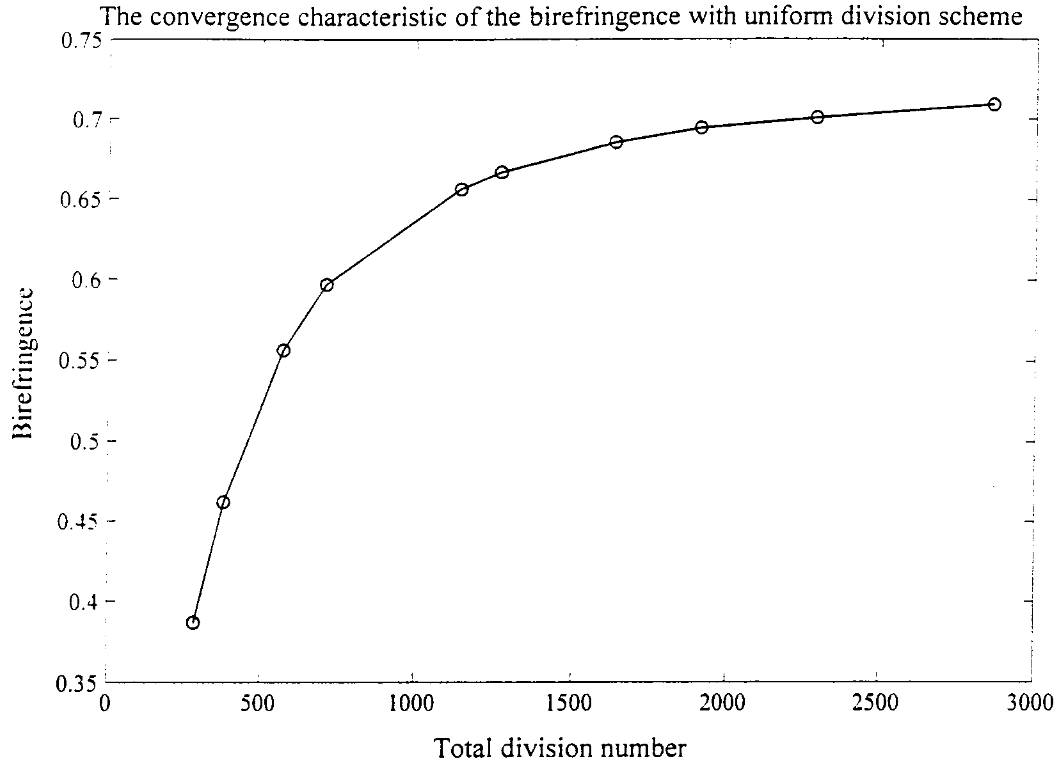

圖(三)　2 × 2融燒式耦合器結構雙折性計算數值隨均勻分割數的收斂情形。

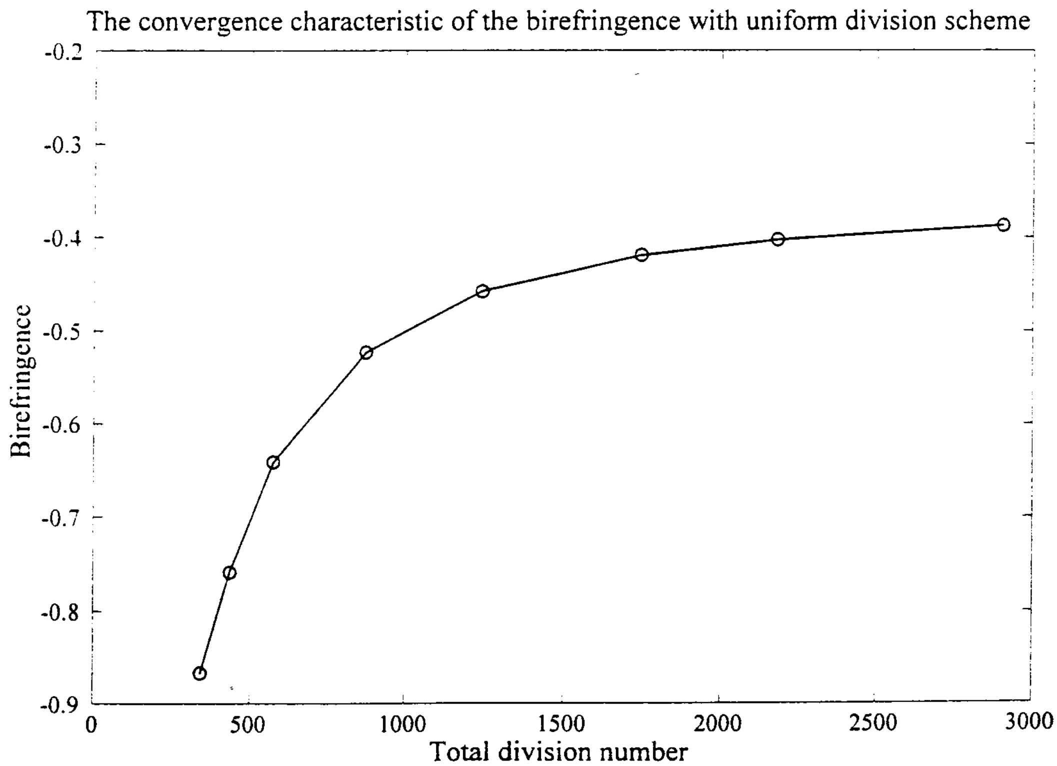

圖(四)　3 × 3融燒式耦合器結構雙折性計算數值隨均勻分割數的收斂情形。

附錄一

Improved Full-Vectorial Finite-Difference Method for Optical Waveguides with Curved Step-Index Profiles

Yen-Chung Chiang, Yih-Peng Chiou, and Hung-chun Chang

Abstract—A rigorous relation, considering a curved interface condition, between a sampled point and its nearby points in the finite-difference analysis of two-dimensional optical waveguides is derived. Our formulation is a full-vectorial one and the interface can be curved with step-index profiles. The validity of the proposed method is proved by comparing our numerical results with the analytical solution of a step-index optical fiber.

Index Terms—Finite-difference method, full vetorial analysis, step-index optical waveguide.

I. Introduction

With the rapid progress of computers, in both software and hardware, a relatively low cost and highly accurate method to design or predict the performance of an optoelectronic device is to make use of the simulation programs or computer-aided design (CAD) tools. Among these CAD tools, the finite-difference method (FDM) is one of the most popular numerical methods, which is widely used in the mode solvers and beam propagation methods (BPMs) because of its simplicity to implement and the sparsity of its resultant matrix.

Although the scalar and the semivectorial analysis methods are easier to implement, they are not accurate enough for such cases with high refractive index contrast in which the coupling between two components of orthogonal polarization is not negligible and a full-vectorial formulation will be needed. Although the current existing FDMs for analyzing two-dimensional structures have claimed the ability of dealing with arbitrary shape of index [1]–[2], most of them cannot deal with structures with oblique or enven curved interfaces properly. We have proposed improved finite difference formulae based on magnetic fields with the oblique interface [3]. It is found that similar formulations based on electric fields cannot fit the curved interface very well, thus new formulae based on electric fields with curved interface would be necessary. In this paper we propose a new finite difference formulation for treating optical waveguides with curved step-index profiles.

II. Formulation

A rigorous relation between the electric fields E_x and E_y at the sampled point (m,n) and the fields nearby, as shown in Fig. 1, will be derived in this section. For more detailed derivation procedure, please refer to our

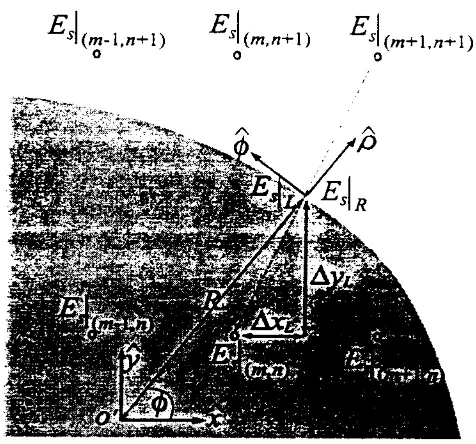

Fig. 1. Cross section of problem under consideration.

prior articles [3], [4]. We assume that there is a curved interface with the normal and tangential unit vectors, $\hat{\rho}$ and $\hat{\phi}$, respectively, as shown in Fig. 1, between the sampled point area and the area with different refractive index. Let the curvature of the interface be κ, or the effective radius be $R = 1/\kappa$. Consider the fields at a sampled point (m,n), denoted as $E_x|_{(m,n)}$ and $E_y|_{(m,n)}$, and the fields nearby, $E_x|_{(m+1,n+1)}$ and $E_y|_{(m+1,n+1)}$ for example, as shown in Fig. 1, and let $E_x|_R$, $E_y|_R$, $E_x|_L$, and $E_y|_L$ represent fields at just to the left and just to the right sides of the interface, respectively. Using the two-dimentional Taylor series expansion, $E_x|_L$ and $E_y|_L$ are expressed as

$$E_s|_L = E_s|(m,n) + \frac{\Delta x_L}{1!}\left.\frac{\partial E_s}{\partial x}\right|_{(m,n)} + \frac{\Delta y_L}{1!}\left.\frac{\partial E_s}{\partial y}\right|_{(m,n)}$$

[1]This work was supported in part by the National Science Council of the Republic of China under Grant NSC89-2218-E-002-093.

Y.-C. Chiang is with the Department of Electrical Engineering, National Taiwan University, Taipei, Taiwan 106-17, R.O.C.

Y.-P. Chiou was with the Department of Electrical Egineering, National Taiwan University. He is now with Rsoft Inc., Ossining, NY 10562, U.S.A.

H.-C. Chang is with the Department of Electrical Engineering, the Graduate Institute of Electro-Optical Engineering, and the Graduate Institute of Communication Engineering, National Taiwan University, Taipei, Taiwan 106-17, R.O.C. (E-mail: hcchang@cc.ee.ntu.edu.tw).

$$+ \frac{\Delta x_L^2}{2!} \frac{\partial^2 E_s}{\partial x^2}\bigg|_{(m,n)} + \frac{2\Delta x_L \Delta y_L}{2!} \frac{\partial^2 E_s}{\partial x \partial y}\bigg|_{(m,n)}$$

$$+ \frac{\Delta y_L^2}{2!} \frac{\partial^2 E_s}{\partial y^2}\bigg|_{(m,n)} + \frac{\Delta x_L^3}{3!} \frac{\partial^3 E_s}{\partial x^3}\bigg|_{(m,n)} + \cdots \quad (1)$$

where s stands for x or y. When (1) is differentiated with respect to x or y, we can express the derivatives of $E_s|_L$ in terms of the derivatives of $E_s|_{(m,n)}$ in a similar manner. These relations can be rewritten in a matrix form denoted as

$$\overline{E}|_L = \overline{\overline{M}}_{L:(m,n)} \cdot \overline{E}|_{(m,n)} + \text{H.O.T.} \quad (2)$$

where $\overline{E}|_L$ represents the vector consisting of $E_x|_L$ and $E_y|_L$ and their derivatives with respect to x and y at just to the left of the interface, $\overline{E}|_{(m,n)}$ represents that consisting of $E_x|_{(m,n)}$ and $E_y|_{(m,n)}$ and their derivatives with respect to x and y, and H.O.T. means high-order terms at the sampled point (m, n). Similarly, $E_s|_{(m+1,n+1)}$ and their derivatives can be expressed in terms of $E_s|_R$ and their derivatives as

$$\overline{E}|_{(m+1,n+1)} = \overline{\overline{M}}_{(m+1,n+1):R} \cdot \overline{E}|_R + \text{H.O.T.} \quad (3)$$

Then we transform the field components and their derivatives with respect to x and y into those in a new local cylindrical coordinate built according to the unit vectors $\hat{\rho}$ and $\hat{\phi}$, and the effective radius R, as shown in Fig. 1, and their derivatives with respect to ρ and ϕ. This transformation can be expressed as

$$\begin{aligned}
E_x &= \cos\phi \cdot E_\rho - \sin\phi \cdot E_\phi \\
E_y &= \sin\phi \cdot E_\rho + \cos\phi \cdot E_\phi \\
\frac{\partial E_x}{\partial x} &= \frac{\sin^2\phi}{R} E_\rho + \cos^2\phi \frac{\partial E_\rho}{\partial \rho} - \frac{\sin\phi\cos\phi}{R}\frac{\partial E_\rho}{\partial \phi} + \\
& \quad \frac{\sin\phi\cos\phi}{R} E_\phi - \sin\phi\cos\phi \frac{\partial E_\phi}{\partial \rho} + \frac{\sin^2\phi}{R}\frac{\partial E_\phi}{\partial \phi} \\
& \vdots
\end{aligned}$$

or in a matrix form

$$\widehat{E}|_L = \overline{\overline{M}}_{CL} \cdot \overline{E}|_L. \quad (4)$$

Likewise, we can transform back to the x-y coordinate system from the ρ-ϕ system in a similar manner as

$$\overline{E}|_R = \overline{\overline{M}}_{RC} \cdot \widehat{E}|_L. \quad (5)$$

The interface conditions require that

$$\begin{aligned}
E_\rho|_R &= \frac{\epsilon_L}{\epsilon_R} E_\rho|_L \\
E_\phi|_R &= E_\phi|_L \\
\frac{\partial E_\rho}{\partial \rho}\bigg|_R &= \frac{\partial E_\rho}{\partial \rho}\bigg|_L + \frac{1 - \epsilon_R/\epsilon_L}{R} E_\rho|_L \\
\frac{\partial E_\rho}{\partial \phi}\bigg|_R &= \frac{\epsilon_L}{\epsilon_R}\frac{\partial E_\rho}{\partial \phi}\bigg|_L \\
\frac{\partial E_\phi}{\partial \rho}\bigg|_R &= \frac{\partial E_\phi}{\partial \rho}\bigg|_L + \frac{(\epsilon_L/\epsilon_R - 1)}{R}\frac{\partial E_\rho}{\partial \phi}\bigg|_L \\
\frac{\partial E_\phi}{\partial \phi}\bigg|_R &= \frac{\partial E_\phi}{\partial \phi}\bigg|_L \\
& \vdots
\end{aligned}$$

or denoted by the matrix form

$$\widehat{E}_R = \overline{\overline{M}}_{RL} \cdot \widehat{E}_L. \quad (6)$$

It is worth noticing that the E_x and E_y components at the interface will be coupled together via the interface conditions. Finally, we can express the fields at nearby points in terms of the fields and their derivatives at the sample point (m, n) as

$$\overline{E}|_{(m+1,n+1)} = \overline{\overline{M}}_{(m+1,n+1)} \cdot \overline{E}|_{(m,n)} + \text{H.O.T.} \quad (7)$$

where

$$\overline{\overline{M}}_{(m+1,n+1)} = \overline{\overline{M}}_{(m+1,n+1):R} \cdot \overline{\overline{M}}_{RC} \cdot \overline{\overline{M}}_{RL} \cdot \overline{\overline{M}}_{LC} \cdot \overline{\overline{M}}_{L:(m,n)}. \quad (8)$$

From these relations connecting the fields and their derivatives at the sampled point with the fields at the nearby points, we can find out a new set of finite difference formulations. And the coupling between E_x and E_y has been included automatically through the above derivation.

III. Numerical Results

To validate the method presented above, we choose a step-index fiber as an example since the exact analytical solutions are known. The parameters we choose for a multimode fiber are as follows: core diameter, d=15 μm; material index, $n_{co} = 1.47$ for the core and $n_{clad} = 1.46$ for the cladding; and the operating wavelength, λ=1.55 μm. These parameters are the same as those used by Xu et al. [5].

We calculate the fundamental HE_{11} mode and the higher order TE_{01} mode and compare with the analytical solutions. The convergence of the numerical solutions is evaluated by reducing the mesh size. Fig. 2 shows the percentage error in the normalized propagation constants of the modes for different mesh sizes. We also plot the results calculated by Xu et al. [5] for comparison. It is noted that, for both the fundamental and the higher order modes, numerical results converge to their exact solutions as the mesh size decreases, and in both cases our results are better than those given in [5]. Figs. 3 and 4 show the plotted patterns of the two transverse electric field components of the HE_{11} mode and the TE_{01} mode, respectively. In the HE_{11} mode case, it is found that the ratio between the two components is over one thousand. Hence, the HE_{11} mode is very close to the scalar LP_{01} mode and can be calculated accurately by either scalar or semivectorial formulation. However, in the TE_{01} mode case the two components have amplitudes of the same order and it cannot be calculated by

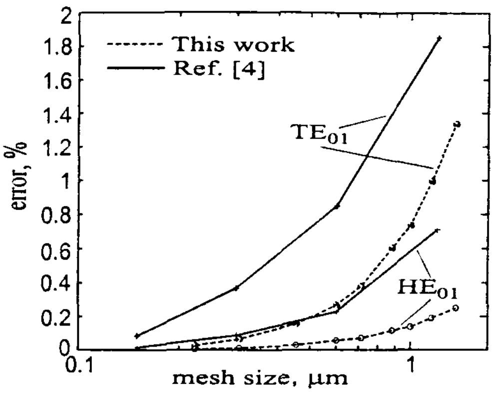

Fig. 2. Percentage error of normalized propagation constants of the HE_{11} and TE_{01} modes of the optical fiber as a function of mesh size $\Delta_x = \Delta_y$.

the scalar or semivectorial method since none of the two components is negligible. All the calculated results are consistent with the exact analytical solutions.

IV. Conclusion

We have derived improved formulae for the finite-difference analysis of two-dimensional step-index waveguides with the curved interface. A rigorous relation is derived from the Taylor series expansion, local coordinate transformation, and matching the interface conditions. The formulation is a full-vectorial one and the only truncation error is not from matching the interface conditions but from the truncation of the higher order terms in the Taylor series expansion. The improved formulation has been applied to calculate the fundamental HE_{11} mode and the higher order TE_{01} mode of a step-index fiber and the results have been compared with exact analytical solutions and those of [5]. It is found that the results converge to the exact analytical solutions and our results are better than those of [5].

References

[1] C. Vassallo, "Improvement of finite difference methods for step-index optical waveguides," *Proc. Inst. Elect. Eng., Pt. J*, vol. 139, pp. 137–142, 1992.

[2] M. S. Stern, "Semivectorial polarised finite difference method for optical waveguides with arbitrary index profiles," *Proc. Inst. Elect. Eng., Pt. J*, vol. 135, pp. 56–63, 1988.

[3] Y.-C. Chiang, Y.-P. Chiou, and H.-C. Chang, "Improved two-dimensional full-vectorial finite-difference method for optical waveguides," *Proc. International Photonic Conference 2000*, vol. I, pp. 357–259, 2000.

[4] Y.-P. Chiou, Y.-C. Chiang, and H.-C. Chang, "Improved three-point formulas considering the interface conditions in the finite-difference analysis of step-index optical devices," *J. Lightwave Technol.*, vol. 18, pp. 243–251, 2000.

[5] C. L. Xu, W. P. Huang, M. S. Stern, and S. K. Chaudhuri, "Full-vectorial mode calculations by finite difference method," *Proc. Inst. Elect. Eng., Pt. J*, vol. 141, pp. 281–286, 1994.

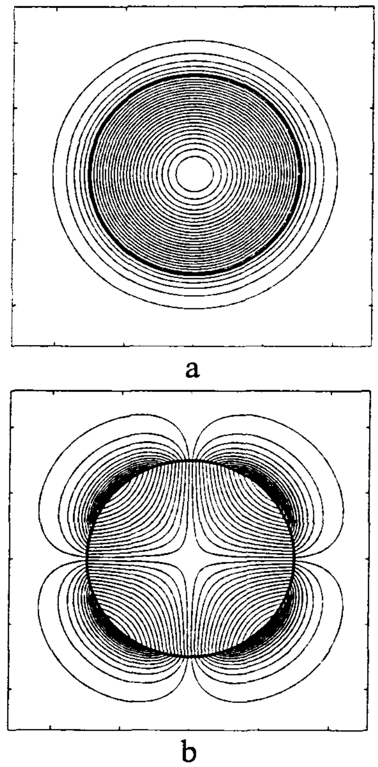

Fig. 3. Field patterns of the fundamental HE_{11} mode of the optical fiber. (a) E_x field and (b) E_y field.

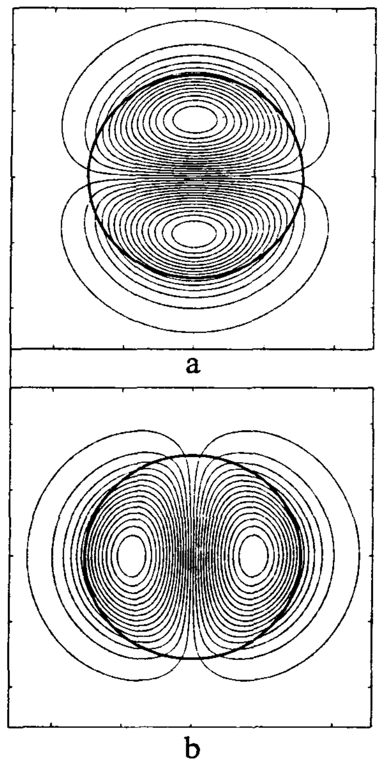

Fig. 4. Field patterns of the fundamental TE_{01} mode of the optical fiber. (a) E_x field and (b) E_y field.

出席國際學術會議報告

民國 91 年 10 月 14 日

會議名稱：國際無線電科學聯合會第二十七屆會員大會(XXVIIth General Assembly, the International Union of Radio Science)

時　　間：2002年8月17日至8月24日

地　　點：荷蘭馬斯垂克會議中心(MECC Maastricht)

發表論文：Chin-ping Yu and Hung-chun Chang, "Research on Photonic Crystal Fibers Using Finite Difference Electromagnetic Analysis"

出席人：　張宏鈞　臺大光電所／電機系教授

計畫編號：NSC90-2215-E002-040

（一）參加會議經過

筆者由國科會專題研究計畫經費補助前往荷蘭馬斯垂克市出席「國際無線電科學聯合會(International Union of Radio Science，簡稱URSI)」的第二十七屆會員大會，並在會中發表論文。URSI的會員大會(General Assembly)，每三年舉行一次，這次的會期是八月十七日至八月二十四日，會場在馬斯垂克會議中心(MECC Maastricht) ，這是歐盟簽約的會場，設備相當不錯。筆者於八月十七日上午飛抵馬斯垂克市，在由阿姆斯特丹至馬斯垂克的班機上恰與中央大學的劉正彥教授同行，他目前擔任URSI中華民國委員會的執行秘書，下機後一同直赴MECC領取會議資料。正式的論文研討會於十九日開始，開幕典禮則於十八日下午四時舉行。開幕典禮進行了近三個小時，除了貴賓致詞外，最重要的節目是頒發每三年一次的van der Pol Gold Medal, J. H. Dellinger Gold Medal, Appleton Prize, 以及Issac Koga Gold Medal等四個獎，本次獲獎者分別是荷蘭Delft Uniersity of Technology的Prof. A.T. De Hoop，史丹福大學的Dr. D. L. Carpenter，加拿大的Prof. S. Haykin，以及比利時Ghent University的Prof. F. Olyslager。其中Dr. D. L. Carpenter係筆者以前在史丹福大學念書時同研究組的師長，早年即以發現地球上空plasmapause的存在而知名，能見到他獲得學術大獎，甚感高興。

URSI共有十個Commissions，所涵蓋的領域從電子元件到太空、無線電天文學的研究，相當廣泛，尤其和電機工程關係相當密切。URSI的會員成員為近五十個各國的委員會，代表中國人的為我國的China/SRS(Taipei)和大陸的China/CIE(Beijing)。根據開幕典禮時的大會報告，本次研討會共將發表772篇口頭報告論文以及741篇壁報論文。我國的出席人員包括China/SRS(Taipei)主席中央大學劉兆漢校長、劉正彥教授、成功大學莊惠

如教授、大同大學黃啟方教授、筆者、及三位青年科學家獲獎人等，約有十餘位。

研討會的論文發表大致以Commission分類，有部分則是兩個以上的Commissions共同規劃的場次，筆者主要參與Commission B (Fields and Waves)以及Commission D (Electronics and Photonics) 的場次，包括Fast Methods for CEM, Numerical Methods for PDEs, Scattering and Diffraction, Electromagnetic Theory, Asymptotic and Hybrid Methods, Optical-Microwave Interactions, Electromagnetic Band Gap Structures and Their Applications, Time Domain Electromagnetics, Nanotechnologic Processes for Advanced Optic and Electronic Systems, Wave Propagation in Fast Photonic Devices等場次，其中有許多論文是由特別邀來的各該領域的著名學者專家所報告，瞭解不同課題的新近發展，收穫良多。在一週的會期中，依照往例，大會安排了三場各一小時的General Lectures，分別邀請三位著名學者專家演講"Radio Science & Cosmology: The Cosmic Microwave Background Radiation," "WHO's Assessment of the Health Effects of EMF Exposure,"及"Synthesizing Optical Frequencies with a Femtosecond Laser"，筆者聆聽了前兩場。另外，各Commission也在不同時段各安排一個一小時的Tutorial，筆者聆聽了Commissions B與D的Tutorials，講題分別是"Inverse Scattering and Its Applications to Sub-Surface Sensing and Medical Imaging"與"Ultra-Fast Photonic Networks Based on Optical Code-Division Multiplexing"。壁報論文場次分別於週二與週四下午四至七時舉行，各有三四百篇論文，場面甚為浩大。

筆者的論文被安排在二十一日下午二時到五時三十分的"Electromagnetic Band Gap Structures and Their Applications"場次發表，這是Commissions B與D的聯合場次，由亞歷桑那大學的Prof. R. W. Ziolkowski與UCLA的Prof. Yahya Rahmat-Samii兩位著名學者所規劃與主持。電磁能隙或光子能隙材料與應用是目前相當熱門的課題，因此吸引不少聽眾，一個不很大的研討室擠滿了八九十位聆聽者，UCLA的Prof. T. Itoh，日本的Prof. H. Ikuno，德國的Prof. Pregla，法國的Dr. Berenger等著名學者也都在場。本場次共安排了九篇論文，前五篇與微波技術相關，後四篇則與光波應用較相關。第一篇論文由Prof. Rahmat-Samii介紹EBG的基本原理及其在微波波段的幾種應用，他是非常好的講者，做了一個很精彩的報告。接著由來自英國、美國、義大利的學者發表他們的研究結果，包括Prof. T. Itoh報告"Left-Handed Transmission Lines and Filters with Low-Loss and Broadband Characteristics"。第六篇論文由Prof. Ziolkowski報告EBG的光波應用，接著有來自土耳其與以色列的兩篇論文，最後由筆者發表與于欽平同學合著的"Research on Photonic Crystal Fibers Using Finite Difference Electromagnetic Analysis" ，這是本場次唯一一篇有關光纖應用的文章，引起好幾位與會者的興趣，問了有關光子晶體光纖應用的問題，筆者詳加回答。參與者眾，討論熱烈，這是相當成功的場次。

筆者二十年前在美國攻讀博士時主要參與URSI中的Commission H "Waves in

Plasmas"主題，回國後的研究則與Commissions B and D較近，但是參加每三年一次的URSI大會總會見到過去的指導教授以及師長們，這次也不例外。閉幕典禮於二十四日中午十二時三十分舉行，筆者因須於二十四日趕回台北，因此提前於二十三日上午搭機離開馬斯垂克返國，無法參與後一天半的研討，不過和筆者研究較相關的文章大致已在前四天發表完畢。

（二）與會心得與建議

光子能隙結構是當今很熱門的研究課題，筆者一直很注意這方面的發展，最近的研究工作也包括光子晶體光纖的分析研究以及光子晶體元件分析方法的開發。在本次研討會我們的光子晶體光纖分析的論文能被安排在EBG的場次，與著名學者一同研討，甚為欣慰。

Commission B在URSI中扮演極為重要的角色，其研究主題，Fields and Waves，雖是古典的領域，但從研討會所發表的論文可以看到歐洲與美國的著名學者們仍兢兢業業努力進行研究，而且有許多優秀的年輕學者加入，是學術氣息相當濃厚的領域。

日本的Prof. H. Matsumoto於1999年大會獲選為URSI會長，筆者在當次的報告中即提到其當選實非偶然，因為日本學者對於URSI的活動相當重視並長時間投入，每次大會均有眾多學者參與，而且在不同Commission均甚活躍，對於各Commission的會長及副會長等職務常多積極爭取，因而累積了競選總會長的實力。從U RSI可看出日本的科技學術實力是全面性的，在各個領域均有學者專家積極投入，今年日本人能分別獲得諾貝爾物理獎與化學獎則為另一佐證。

（三）攜回資料名稱及內容

1. XXVIth General Assembly Abstracts, 光碟片。
2. Review of Radio Science 1999—2002, Edited by W. Ross Stone, 光碟片。
3. Programme, Oral Presentations, International Union of Radio Science, XXVIIth General Assembly, 共228頁。
4. Programme, Poster Presentations, International Union of Radio Science, XXVIIth General Assembly, 共176頁。
5. Opening Ceremony and Presentation of Awards, International Union of Radio Science, XXVIIth General Assembly, 共40頁。

RESEARCH ON PHOTONIC CRYSTAL FIBERS USING FINITE DIFFERENCE ELECTROMAGNETIC ANALYSIS

Chin-ping Yu(1) **and** **Hung-chun Chang**(2)

(1) *Graduate Institute of Communication Engineering,*
National Taiwan University, Taipei, Taiwan 106-17, Republic of China
E-mail: f86025@ew.ee.ntu.edu.tw

(2) *Department of Electrical Engineering, Graduate Institute of Electro-Optical Engineering,*
and Graduate Institute of Communication Engineering
National Taiwan University, Taipei, Taiwan 106-17, Republic of China
E-mail: hcchang@cc.ee.ntu.edu.tw

ABSTRACT

Photonic crystal fibers (PCFs) are one successful application of the photonic crystal concept. We report on analysis and design of the PCFs using the finite difference mode solver. The full-vectorial characteristics of PCFs, including the effective indexes and field distributions of the guided modes, are obtained. Both PCFs based on the total internal reflection guiding mechanism ("holey fibers") and those resulting from photonic bandgap effect have been studied. For the holey fibers, the dispersion property is calculated and is shown to agree very well with experimental values. The vectorial modes on PCFs with a large air core are accurately analyzed.

INTRODUCTION

Photonic crystal fibers (PCFs) or microstructured fibers are novel photonic structures that represent one successful application of the photonic crystal concept [1], [2]. In recent years many research efforts have been devoted to understanding the propagation characteristics of such fibers, based on different theoretical methods [3]–[6], and to demonstrating their possible applications. In this paper we report on analysis and design of the PCFs using the finite difference mode solver. We demonstrate that the full-vectorial finite difference method that has often been employed to study waveguide modes of various dielectric waveguides [7] can be efficiently used to obtain the propagation characteristics, including the effective indexes and field distributions, of different PCFs.

The first PCF reported in 1996 [1] was made from undoped fused silica having a hexagonal array of air holes along its length, with the central hole missing, forming a core area. The scanning electron microscopic (SEM) picture and the cross-section of a typical PCF are shown in Fig. 1(a) [8] and (b), respectively. It was understood that light can be guided

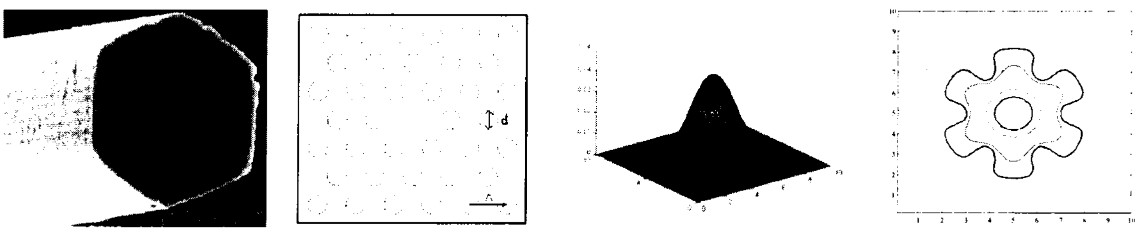

(a) (b) (c) (d)

Fig. 1. (a) SEM picture of the PCF [8]. (b) The cross-section of the PCF. (c) The field distribution and (d) the transverse field distribution for the x-polarized guided mode of the PCF at $\lambda = 0.6328$ μm with $d = 0.6$ μm.

on such structure because the refractive index of the core area is higher than the effective index of the surrounding air-hole array, making the required total internal reflection possible. One peculiar feature of the PCF is that it can maintain as a single-mode guide over a wide wavelength range, called "endlessly single-moded" [2]. In contrast to the

†This work was supported in part by the National Science Council of the Republic of China under Grant NSC90-2215-E-002-040.

effective total internal reflection guiding of the holey fibers, light guiding in the core area due to the existence of photonic bandgaps (PBGs) in the cladding region has been achieved in PCFs in which the core index is made smaller than the effective index of the cladding region [9], and even in PCFs with a large air core [10]. Vectorial modes of all these fibers will be calculated and discussed in this paper.

THE FINITE DIFFERENCE MODEL

Starting from Maxwell's equations, the vector wave equation in a linear, isotropic, and time-invariant medium is derived as

$$\nabla \times \nabla \times \vec{E} = \nabla(\nabla \cdot \vec{E}) - \nabla^2 \vec{E} = n^2 k_0^2 \vec{E} \tag{1}$$

where n is the refractive index as a function of position, and $k_0 = 2\pi/\lambda_0$ is the wave number in free space. For the refractive index does not vary along the z direction, the propagation of the electromagnetic wave is governed by two coupled equations for E_x and E_y only. By writing the electric field as $\vec{E} = (E_x\hat{x} + E_y\hat{y} + E_z\hat{z})\exp(-j\beta z)$, where β is the propagation constant, and considering only the transverse part of the field, we can obtain an eigenvalue equation of the form [11]

$$\begin{bmatrix} A_{xx} & A_{xy} \\ A_{yx} & A_{yy} \end{bmatrix} \cdot \begin{bmatrix} E_x \\ E_y \end{bmatrix} = \beta^2 \begin{bmatrix} E_x \\ E_y \end{bmatrix}. \tag{2}$$

The cross-section of a PCF is then discretized into many mesh points with the above Maxwell differential equations using the central difference scheme to form a set of elementary matrix equations. The effective indexes of the guided modes are obtained by finding out the eigenvalues of the matrix equations, and the field distributions from solving for the eigen vectors. Since the guided modes are found well centrally confined, the computational window is not necessarily large and the transparent boundary condition [11] has been utilized at its boundary.

NUMERICAL RESULTS

We first analyze the PCF that has the radius of the core region equal to Λ , the distance between two air hole centers. The field distribution in the PCF is shown in Fig. 1(c) and (d) at $\lambda = 0.6328$ μm with $d = 0.6$ μm, where d is the air hole diameter. The field is seen to be confined very well in the core area for the air holes reduce the refractive index of the cladding region. Smaller holes also make single-mode guidance more likely. Fig. 2(a) shows the mode indexes of the guided modes versus the normalized frequency with $d/\Lambda = 0.3$. There are actually two modes with different polarization states, which are too close to be distinguished from each other in the figure. The PCF is thus considered as single-moded over a remarkably large band of frequency. Our result agrees very well with previous experimental results [2]. If we further increase the hole diameter, the gaps between the holes become narrower, isolating the core more strongly from the silica in the cladding. Thus, there will be more guided modes in the PCF, as shown in Fig. 2(b) with $d/\Lambda = 0.5$.

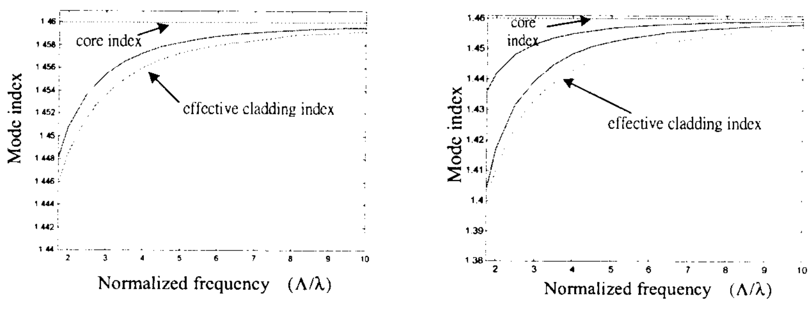

Fig. 2. Modal dispersion curves for (a) a single-mode PCF with $d/\Lambda = 0.3$ and (b) a multimode PCF with $d/\Lambda = 0.5$.

Fig. 3(a) shows the transverse field distribution of the guided mode in the PCF with $d = 1.4$ μm at $\lambda = 0.6328$ μm. Compared with Fig. 1(d), we can see that the field is more centrally located for larger air-hole diameter for it reduces more the cladding index, increasing the index difference between the core and cladding regions. At shorter wavelengths the field becomes more concentrated in the silica regions and avoids the holes as shown in Fig. 1(d) at $\lambda = 0.6328$ μm. As for larger wavelengths, the field will extend more into the holes and the cladding region, as shown in Fig. 3(b) at $\lambda = 1.55\ \mu$m.

The dispersion properties can also be obtained by calculating the effective indexes n_{eff} of the guided modes over a range of wavelength. The actual index of the pure silica is taken into account by means of four-term Sellmeier formulae [12], [13]. The dispersion is derived according to the definition $D = -\lambda d^2 n_{eff}/cd\lambda^2$ considering both the material and the waveguide dispersions. Fig. 4 presents the dispersion characteristics of the PCFs with different air-hole diameters while Λ is set to be 2.3 μm. Note that in our computation for the case with $d = 0.621\ \mu$m and $\lambda = 0.813\ \mu$m, the dispersion is -74.5 ps/nm/km and its slope is 0.472 ps/nm-km/nm, whereas the experimental values in [8] were -77.7 ps/nm/km and 0.464 ps/nm.km/nm, respectively [14]. Our results have very good agreement with the experimental values, showing the reliability of our model. We can also see that the zero-dispersion point can be easily shifted to desired wavelength by changing the geometrical parameters of the PCFs.

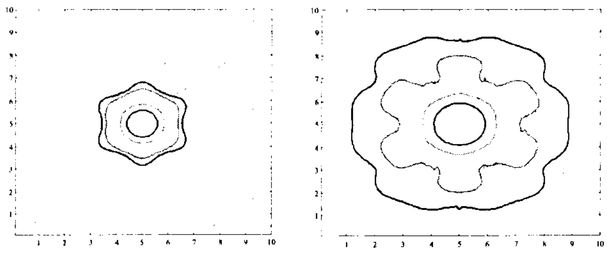

(a) (b)

Fig. 3. The transverse field distribution for the x-polarized guided mode of the PCF at (a) $\lambda = 0.6328\ \mu$m with $d = 1.4\ \mu$m, and (b) $\lambda = 1.55\ \mu$m.

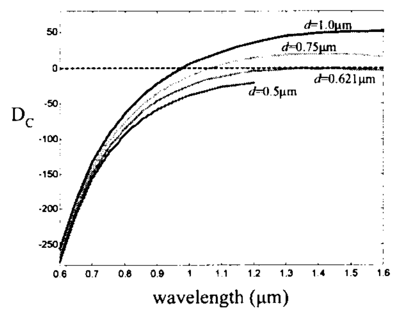

Fig. 4. Dispersion computed versus wavelength for PCFs with different air-hole diameters.

We now consider PCFs with light guiding in the core area due to the existence of PBGs in the cladding region. Fig. 5(a) [9] shows an example of such PCFs, called the honeycomb PCF, which has a smaller air-hole defect in the fiber center resulting in a decrease of the core index. The circles in Fig. 5(b) are the fundamental guided mode indexes on the honeycomb PCF obtained by our model with dashed lines being the boundaries of the PBGs, and the dotted line being the radiation line. The solid line is obtained by the plane-wave expansion method [4], and the triangles are obtained by the FDTD method [6]. Our results appear to be closer to those of the plane-wave expansion method. Another example is the vacuum or air waveguide, as shown in Fig. 6(a) [10]. The core region is filled with air, resulting from removing seven silica glass capillary canes in the fabrication. The fundamental guided modes for $\lambda = 0.55\ \mu$m and $\lambda = 0.65\ \mu$m are shown in Fig. 6(b) and (c), respectively. The field is confined very well in the core area at $\lambda = 0.55\ \mu$m even when the index of the cladding is larger than the index of the core which is equal to 1. The calculated effective mode index is 0.9994993. At $\lambda = 0.65\ \mu$m, the field is seen to spread into the cladding region.

CONCLUSION

We have demonstrated that the finite difference method is an efficient method for studying PCFs. The characteristics of various PCFs, including the effective indexes and the field distributions of the vectorial guided modes, have been calculated and discussed. Dispersion properties of the PCFs can also be obtained by our model, and those for the holey fiber are shown to agree very well with the reported experimental values. We have also successfully analyzed PCFs resulting from pure PBG mechanism.

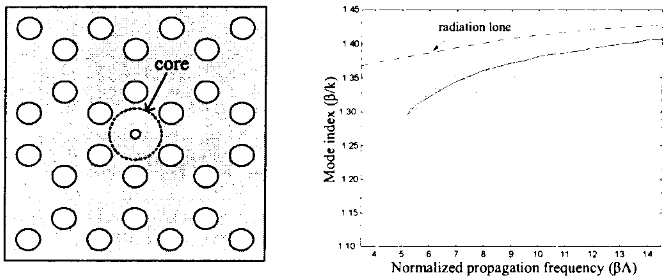

(a) (b)

Fig. 5. (a) Geometry [9] and (b) the fundamental guided mode index of the honeycomb PCF.

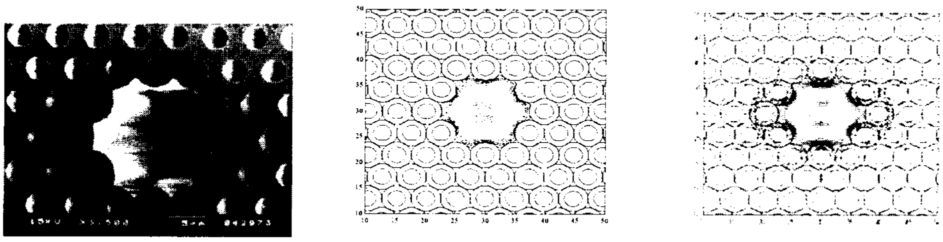

(a) (b) (c)

Fig. 6. (a) SEM picture of a vacuum-guiding PCF [10]. (b) The transverse field distribution for the fundamental guided modes of the vacuum-guiding PCF at $\lambda = 0.55$ μm. (c) Same as (b) but at $\lambda = 0.65$ μm.

REFERENCES

[1] J. C. Knight, T. A. Birks, P. St. J. Russel, and D. M. Atkin, "All-silica single-mode optical fiber with photonic crystal cladding," *Opt. Lett.*, vol. 21, pp. 1547–549, 1996.

[2] J. C. Knight, T. A. Birks, and P. St. J. Russel, "Endlessly single-mode photonic crystal fiber," *Opt. Lett.*, vol. 22, pp. 961–963, 1997.

[3] T. M. Monro, D. J. Richardson, N. G. R. Broderick, and P. J. Bennett, "Holy optical fibers: An efficient modal model," *J. Lightwave Technol.*, vol. 17, pp. 1093–1102, 1999.

[4] S. E. Barkou, J. Broeng, and A. Bjarklev, "Silica-air photonic crystal fiber design that permits waveguiding by a true photonic bandgap effect," *Opt. Lett.*, vol. 24, pp. 46–48, 1999.

[5] F. Brechet, J. Marcou, D. Pagnoux, and P. Roy, "Complete analysis of the characteristics of propagation into photonic crystal fibers, by the finite element method," *Opt. Fiber Technol.*, vol. 6, pp. 181–191, 2000.

[6] M. Qiu, "Analysis of guided modes in photonic crystal fibers using the finite-difference time-domain method," *Microwave and Optical Technol. Lett.*, vol. 30, pp. 327–330, 2001.

[7] Huang, W. P., and C. L. Xu, "Simulation of three-dimentional optical waveguides by a full-vector beam propagation method," *IEEE. J. Quantum.*, vol. 29, pp. 2639–2649, 1993.

[8] Homepage of the Optoelectronics Group, Department of Physics, University of Bath.

[9] J. C. Knight, J. Broeng, T. A. Birks, and P. St. J. Russell, "Photonic band gap guidance in optical fibers," *Science*, vol. 282, pp. 1476–1478, 1998.

[10] R. F. Cregan, B. J. Mangan, J. C. Knight, T. A. Birks, P. St. J. Russell, P. J. Roberts, and D. C. Allan, "Single-mode photonic band gap guidance of light in air," *Science*, vol. 285, pp. 1537–1539, 1999.

[11] G. R. Hadley, "Transparent boundary condition for the beam propagation method," *IEEE J. Quantum Electron.*, vol. 28, pp. 963–970, 1992.

[12] B. Brixner, "Refractive-index interpolation for fused silica," *J. Opt. Soc. Amer.*, vol. 57, pp. 674–676, 1967.

[13] I. H. Maliston, "Interspecimen comparison of the refractive index of fused silica," *J. Opt. Soc. Amer.*, vol. 55, pp. 120–1209, 1965.

[14] M. J. Gander, R. McBride, J. D. C. Jones, D. Mogilevtsev, T. A. Birks, J. C. Knight, and P. St. J. Russel, "Experimental measurement of group velocity dispersion in photonic crystal fibres," *Electron. Lett.*, vol. 35, pp. 63–65, 1999.